Digital mapping of soil salinity at various depths using an EM38

Bhaskar Narjary[1]*, M.D.Meena[1], Satyendra Kumar[1], S.K.Kamra[1], D.K.Sharma[1] and J. Triantafilis[2]

[1]Central Soil Salinity Research Institute, Karnal-132001, Haryana, India

[2] University of New South Wales - School of Biological, Earth and Environmental Sciences, New South Wales, Australia

*Corresponding Author's details:

Dr. Bhaskar Narjary, Central Soil Salinity Research Institute, Karnal-132001, Haryana, India

E-mail: bhaskar.narjary@gmail.com

Alternate E mail: bhaskar.narjary@icar.gov.in

Running title: Soil salinity mapping using EM38

Abstract

Problem definition: Spatial information on salinity is required at the farm level to enable suitable soil, crop and water management practices. Rationale: To facilitate this, we used an electromagnetic (EM) induction instrument for rapid measurement of apparent soil electrical conductivity (EC_a – mS/m) across the 11 ha area of the Central Soil Salinity Research Institute (CSSRI) experimental farm in Nain, Haryana, India. Methods: The EC_a was measured using an EM38 in horizontal (EC_{ah}) and vertical (EC_{av}) modes on a grid survey. Using the EC_a data we selected 21 locations using the response surface sampling design (RSSD) module of Electrical Conductivity Sampling Assessment and Prediction (ESAP) software. We collected soil samples at four depth increments, including two topsoil (0-0.15 m and 0.15-0.30 m), a subsurface (0.3-0.6) and a subsoil (0.6-0.9) and measured the soil electrical conductivity (EC_e-dS/m). Results: We developed multiple linear regression (MLR) to predict EC_e using the ESAP software from EC_{ah} and EC_{av} and two-trend surface parameters (i.e. Easting and Northing) across the farm. The prediction accuracy and bias were compared at different depth increments and results of the spatial distributions of EC_e using ordinary kriging (OK) interpolation were described in terms of the crop and soil use and management implications. Conclusions: We conclude the overall approach allows for generations of a digital soil maps (DSM) of EC_e and which serve as baseline data that will allow the monitoring of any rehabilitation effort of salt-affected soils according to their actual degree of salinity.

Keywords: EM-38, ESAP, Soil salinity, Ordinary kriging

Digital mapping of soil salinity at various depths using an EM38

Introduction

Soil salinity is a serious environmental problem which adversely affects crop yield, soil health and socio-economic conditions of the farming communities in the Indo-Gangetic plain. This is particularly the case in the semi-arid north-western Indian states of Haryana, Punjab, Rajasthan and Gujarat, where salinization results from the presence of naturally occurring salt bearing minerals (halite, Kumar *et al*., 2010) in the soil. Secondary salinity arises because of the development of irrigation through extensive canal systems and owing to poor water management, waterlogging and shallow saline water tables which develop across the flat alluvial landscape. Driven by strong evaporative demand, the salt is brought to the surface through capillary rise. The problem is exacerbated in irrigated areas having inadequate drainage. As a result, salinity seriously threatens the sustainability of irrigated agriculture of North West India across 2 million ha (Kamra, 2015). There is a need to characterise the spatial distribution of salinity at farm level to understand extent and determine the most appropriate soil, water and crop management to return to agricultural productivity. It is also required to gauge management against baseline soil salinity.

However, traditional laboratory methods of determining salinity, such as the electrical conductivity of a saturated soil paste extract (e.g. EC_e) are labour intensive, time consuming, and expensive (Traintafilis *et al*., 2012) and only provide point information. It has been shown that the use of electromagnetic (EM) induction instruments can be used as ancillary data to rapidly map soil properties relevant to salinity. This is because EM instruments measure the apparent soil electrical conductivity (EC_a), which is a function of properties such as clay (Saey *et al*., 2009), mineralogy (Nagra *et al*., 2017) and moisture (Brevik *et al*., 2006). More importantly,

66 when these properties are uniform across a study site (Friedman, 2005), the shallow measuring
67 EM38 instrument has been used to first enable site selection for calibration (Triantafilis *et al*.,
68 2000) and subsequently for mapping salinity at field (Li *et al*., 2013), across farms (Buchanan
69 and Triantafilis, 2009) and landscapes (Odeh *et al*., 1998). This includes the use of mechanized
70 mobilized sensing systems where large amounts of EC_a data are collected quickly at the field
71 scale and which have been used to investigate salinity in southwest USA (Rhoades *et al*., 1999;
72 Cassel *et al*., 2015), Australia (Huang *et al*., 2014), Spain (Herrero *et al*., 2011) and increasingly
73 in China (Li *et al*., 2012). However, there are limited case studies where this type of research has
74 been undertaken in developing countries; Pakistan (Chaudhary and Baig, 2000), India (Banerjee
75 *et al*., 1998; Narjary *et al*., 2017) and Bangladesh (Aziz *et al*., 2008)

76 Owing to the success of these researchers, we use a similar approach but using an EM38
77 on a grid and across the Central Soil Salinity Research Institute (CSSRI) experimental farm in
78 Nain, Haryana, India. In the first instance we measure the apparent electrical conductivity (EC_a)
79 in horizontal (EC_{ah}) and vertical (EC_{av}) modes. We then use the US Salinity Laboratory
80 Electrical Conductivity Sampling Assessment and Prediction (ESAP) software (Lesch *et al*.,
81 2000) to choose appropriate soil sampling locations using the response surface sampling design
82 (RSSD) module. Four multiple linear regression (MLR) equations were used for predicting soil
83 salinity (EC_e) in two top soil (0-0.15m and 0.15-0.3 m), a subsurface (0.3-0.6m) and a subsoil
84 (0.6-0.9) depth using the two EC_a measurements and trend surface parameters (Easting and
85 Northing). We discuss the prediction accuracy and bias of prediction at the different depth
86 increments. The study also aims to develop spatial salinity maps and confer maps in terms of
87 crop and soil use and management implications with respect to effect of salinity on soil health
88 and agricultural productivity.

Material and Methods

Experimental site

The study site is located on the Central Soil Salinity Research Institute farm near Nain, which is located in the Panipat district of Haryana State, India. The farm is 11 ha in size and geographically extends between 29°19'7.09" to 29°19'10"N latitude and 76°47'30.0" to 76°48'0.0"E longitude (Fig. 1). It is at an elevation of 213-214 m above mean see level. The study farm falls within the QIG2 geomorphic surface (Shrivastava *et al*., 2015) and the soil is characterised by a sandy loam texture and according to USDA (United States Department of Agriculture) soil taxonomy classified as mixed Typic haplustepts (saline phase) (Sachdev *et al*., 1995; Mondal *et al*., 2013).

Climatically the farm is situated in a sub-tropical and semi-arid climate with average annual rainfall of 550-650 mm. The rainfall (77 %) occurs during south-west monsoon (i.e. July to mid-September) and about 1,500 mm annual evaporation under a *Ustic* soil moisture regime (Mandal *et al*., 2013). During the summer months (March-May) mean maximum temperature ranges between 30-39 °C and mean minimum temperature ranges 18-27 °C.

The site had been lying barren for nearly two decades due to salinization and owing to the presence of a shallow perched water table (~1 m), particularly during the wet monsoon months. The water table is deeper (~3.5 m) during the summer. Before being acquired by the CSSRI in 2011, the land was a part of village community land and was abandoned for a long period of time. This led to the emergence of naturally growing trees, bushes and shrubs commonly found in salty land with poor quality (saline) groundwater. Though the vegetation type and density varied spatially, the dominant species were *Prosopis juliflora* (Babool), *Azadirachta indica*

(Neem), *Ziziphus numularia* (Jharberi) and *Dalbergia sissoo* (Sisham). The farm also has salt tolerant grasses and herbs; including, *Saccharum spontanium* (Kans), *Cynodon dactylon* (Dub grass), *Suaeda fruticosa* (Noon-khari), *Kochia indica* (Bui) and *Calotropis procera* (Aak).

After acquiring the farm, these naturally growing trees, bushes and grasses were removed. The land was leveled, and the soil leached through monsoon rain water by dividing the farm into a number of fields using dykes. The main land use in the monsoon is cultivation for Pearl millet (*Pennisetum glaucum*) and in winter season is mustard (*Brassica juncea*). Some part of the landscape is dedicated to agro-forestry of *Eucalyptus*.

EM Survey

An analogue EM38 (Geonics Limited, Mississuaga, Canada) was used to undertake EC_a survey across the CSSRI Nain Experiment farm in the summer month of May 2013. Two EC_a measurements were collected (i.e. EC_{ah} and EC_{av}). A total of 276 measurement sites were visited along transects spaced ~15-20 m apart (Fig. 2a). A Global Positioning System (GPS) was used to identify the exact location of each measurement site. Trimble GEO XT GPS system was used to record two trend surface parameters i.e. Easting and Northing.

A contour survey analysis of the farm was carried out using dumpy level (Optical instrument used to establish or verify points in the same horizontal plane). We found that the farm was fairly level (Fig. 2b), ranging between 212.99 to 213.67 m above mean sea level. Higher elevation was observed in the southeast corner where a farm pond has been excavated and excavated soil has been stacked over the land. The lowest elevation was observed in the middle of the farm from the south east side.

135 **Collection of soil samples and laboratory analysis**

136 To enable calibration between EM38 EC_a and EC_e and to understand relationships with
137 various soil properties and dominant salts, soil samples were collected simultaneously from
138 selected EM38 measurement sites. Response Surface Sampling Design (RSSD) module of the
139 EC_e Sampling, Assessment and Prediction (ESAP) software package was used to select locations
140 based on the EC_a data (Lesch *et al*., 2000). In brief, the design involves de-correlating EC_a using
141 a principal component transformation. This transformed data is then directly compared to a
142 suitable RSSD composed of n design level combinations balanced across m principal component
143 vectors.

144 The aim of the RSSD is to select a small set of sampling sites to optimise estimation of
145 regression parameters for predicting soil properties with ordinary least squares estimation
146 approach and to minimise effects of the spatially dependent error structure on the estimation
147 process (Triantafilis and Lesch, 2005). In practical terms, this led to the selection of EM38 (EC_{ah}
148 and EC_{av}) values at low (< 100 mS/m), intermediate-low (100-200 mS/m), intermediate (200-350
149 mS/m), intermediate-high (350-500 mS/m) and high (>500 mS/m) with sites spread across the
150 farm. Fig. 2b shows the location of the 21 soil sampling locations.

151 At each of the 21 sites, samples up to a depth of 0.90 m were collected at the depth
152 increments of two topsoil (0-0.15 m and 0.15-0.30 m), a subsurface (0.3-0.6) and a subsoil (0.6-
153 0.9). Since soil texture and moisture content are reported to be important variables influencing
154 calibration of EM observations with EC_e (McKenzie *et al.*, 1989; Vaughan *et al.*, 1995), one
155 portion of the soil sample was collected in aluminum moisture box for determination of
156 gravimetric moisture content (GMC), and saturation percentage (SP). This is because SP is
157 closely related to soil texture (Lesch *et al.*, 2000). For chemical analysis, the soil samples were

air dried, ground and passed through a 2-mm sieve and analyzed for the electrical conductivity of a saturated soil paste extract (EC_e- Eutech EC meter), soluble cations (Ca^{2+} and Mg^{2+}) and anions (CO_3^{-2}, HCO_3^{-1} and Cl^{-1}) using a wet chemistry (Titration) procedure (Bhargava, 2003), Na^{+1} and K^{+1} ions determined using a flame photometer (Systronics India Limited).

Understanding EC_e and Modeling of EC_a data

For correlating EM38 observations (EC_{ah} and EC_{av}) with EC_e at various depth increments an MLR model software package (ESAP) was used and which considers both EC_a and two trend surface parameters (i.e. Easting [x] and Northing [y]) of each survey site. The prediction variable, Y is derived in this model as per the following equation:

$$Y=b_0+ b1\,(EC_{ah}) +b2\,(EC_{av}) +b3(x) +b4(y)\ldots\ldots\ldots\ldots\ldots\ldots(1)$$

Where EC_{ah} and EC_{av} represent the EM38 observations in horizontal and vertical orientations, x and y represent the spatial coordinates of EM38 locations, while *bo*, *b*1, *b*2, *b*3, and *b*4 are fitted model parameters. To circumvent co-linearity, transformed and uncorrelated principal component scores were used in place of the raw EM38 observations as predictor variables, while scaling techniques of the surface parameters are used to increase the prediction accuracy in the MLR model (Lesch *et al.*, 1995b). Consequently, the depth specific MLR prediction model can be represented as:

$$Y = b_0 +b_1\,(z_1) + b_2\,(z_2) + b_3\,(u) +b_4\,(v)\ldots\ldots\ldots\ldots\ldots\ldots(2)$$

Where z_1 and z_2 are the de-correlated EM38 observations (i.e., the principal component scores) and (u, v) represent the scaled spatial coordinates of each survey site (Lesch *et al.*, 2000).

Statistical Analysis

The performance of the model was evaluated by using statistical tools such as the R^2 (coefficient of determination), root mean square error (RMSE), model efficiency (ME) and Wilmot's index of agreement (IoA). Statistical analysis was done using Excel and online with SAS 9.2 version (http://stat.iasri.res.in/sscnarsportal).

Geo-statistical analysis of spatial variability

Ordinary kriging (OK) was used to characterize the variance structure, determination of spatial distribution, and trend changes of soil properties. The OK method uses a semi-variogram to quantify the spatial dependence between neighbouring observations. Four types of semi-variogram models (Circular, Spherical, Exponential, and Gaussian) were tested using geo-statistical modules in Arc-GIS 9.3 (Arc-GIS, 2008). For the selection of the best model, predictive performances of the fitted models were checked on the basis of a leave-one-out-cross-validation test. Herein we used point kriging. Values of Mean Standardized Error (MSE), Root Mean Square error (RMSE), Average Standard Error (ASE) and Root Mean Square Standardized error (RMSSE) were estimated to ascertain the performance of the fitting models (Gorai *et al*., 2017).

Results and Discussion

Spatial distribution and descriptive statistics of EC_a

Table 1 shows the descriptive statistics of measured EC_{ah} and EC_{av}. In terms of the shallower measuring EC_{ah}, it had a smaller mean (358.3 mS/m) but larger standard deviation (182 mS/m) than the deeper measuring EC_{av} (404.7 and 162 mS/m, respectively). These results were a function of the larger range in EC_{ah} (917 mS/m) from a minimum of 45 mS/m to a

maximum of 962 mS/m, compared with the EC_{av} which varied from 58 to 771 mS/m. This suggests that in some parts of the study area, EC_e may be larger in the topsoil layers as compared to the subsoil; representing inverted salinity profiles.

Nevertheless, and as indicated by the kurtosis value for both EC_{ah} (-0.4) and EC_{av} (-0.7), which were both less than 3, the distributions were platykurtic. This implies the distributions have fewer and less extreme outliers than a normal distribution. The histograms shown in Fig.3a and 3b, show that the EC_{ah} and EC_{av} respectively, were normally distributed and symmetric with well-behaved tails. Given the skewness of the EC_{ah} (0.5) and EC_{av} (0.1) were also small; no transformation was required for further analysis of the measured EC_a survey data.

Table 1 also shows the descriptive statistics of the EC_a measurements at the 21 calibration sites. For the most part, the mean and median and other statistics are equivalent with those achieved with the survey data, with similar values of skewness and kurtosis in the two data sets. This indicates that the calibration data is a fair reflection of the survey data. The spatial distribution shown in Fig. 2b also shows that the calibration sites are evenly distributed across the farm.

Fig. 4a shows the variation in EC_{ah} as a contour plot (JMP Version 12). It was evident that the smallest EC_{ah} (< 200 mS/m) was measured along the western and southern margins. Conversely, and with increasing distance to the eastern side, EC_{ah} increases whereby the largest measurements (> 600 mS/m) are adjacent to a large pond located in the centre of the farm. The pattern in EC_{av} was equivalent except it appeared to be universally intermediate-large (i.e. > 600 mS/m) across the farm (Fig. 4b). The area of large EC_a was more extensive and consistent with areas where water-logging was problematic in the eastern half and southern parts of the farm. In both cases, there was a trend in EC_a with Easting and Northing, respectively.

226

227 **Descriptive statistics of measured soil properties**

228 Table 1 also shows the descriptive statistics at various depths of the measured properties
229 (EC_e, SP and GMC). With respect to EC_e, the salinity varied from non-saline (< 2 dS/m) at all
230 depths to highly-saline (> 32 dS/m). This was particularly the case in the topsoil (0-0.15 m) and
231 subsurface (0.15-0.30 m) where salinity was largest (respectively, 50.8 and 41.5 dS/m). Given
232 the slightly smaller EC_e maximums in the subsoil, this suggests the process driving salinization
233 was a rising water table and accumulation of salts in the topsoil through capillary rise and high
234 evaporative demand. This was a function of the semi-arid nature of the area which was
235 influenced by monsoonal weather patterns.

236 Of the other soil properties which influence EM38 EC_a there appears to be little variation
237 in these. With respect to soil texture, the small range in SP at various depths suggests there is
238 little variation in soil texture. The uniform and small range in GMC at the various depths
239 indicates little variation in soil moisture; it was a drier in the topsoil (14.4 %) than in the deepest
240 subsoil (19.9 %).

241

242 **Linear- and multiple-linear regression analysis**

243 Table 2 shows there was significant positive correlation between EC_{ah} and EC_{av} and
244 average profile (0-0.90 m) EC_e of 0.76 and 0.74 ($p < 0.01$), respectively. This was not the case
245 with respect to many of the other average profile properties measured including SP (-0.02), GMC
246 (-0.23), Ca + Mg (0.37) and CO_3^{-2} + HCO_3^{-1} (-0.21) which were poorly correlated. In terms of
247 the poor correlation with SP this suggests that the soil texture across the farm was relatively

248 uniform. This was similarly the case with GMC, which indicates soil moisture was consistent at
249 the time the EM38 survey was conducted.

250 However, there was a large positive correlation (> 0.7) for both EC_{ah} and EC_{av} with some
251 of the cations (Ca^{2+}, Mg^{2+}, Na^{+}) and anions (CO_3^{2-}, HCO_3^{-}, Cl^{-}). The largest correlations were for
252 Na (0.77 and 0.74, respectively) and Cl (0.73 and 0.71, respectively). Along with the fact that
253 these ions were strongly correlated with EC_e, this indicates that sodium chloride (NaCl) was the
254 major salt responsible for EC_e in the study area and which contribute most to EC_a variation.

255 Table 3 shows the multiple linear regression (MLR) summary statistics derived from
256 model (eq. 2) using EC_{ah} and EC_{av} and to predict EC_e at non-sampled points (i.e. locations where
257 only EC_{ah} and EC_{av} data were collected) and for the two topsoil (0-0.15 m and 0.15-0.30 m),
258 subsurface (0.3-0.6) and a subsoil (0.6-0.9) depth increments of interest. The largest (0.86) R^2 for
259 a calibration was achieved for the upper topsoil (0-0.15 m) MLR model to predict EC_e, with
260 reasonable RMSE (6.36 dS/m) (Table 1).

261 The MLR model for lower topsoil (0.15-0.30 m) and subsurface (0.3-0.6 m) were also
262 good, although slightly smaller R^2 (i.e. 0.77 and 0.78, respectively). While the RMSE were also
263 equivalent (i.e. 6.32 and 5.96 dS/m, respectively), the model efficiency was slightly smaller (i.e.
264 0.77 and 0.72, respectively) owing to the smaller standard deviations (SD) in EC_e (i.e. 11.9 and
265 11.3 dS/m, respectively) as compared with the topsoil (15.1 dS/m).

266 The MLR model for the subsoil (0.6-0.9 m) was reasonable, although the R^2 (0.66) was
267 smaller again than the lower topsoil and subsurface depths. We attribute this to various factors.
268 In terms of the EC_e it was because the range in EC_e was smallest for this depth increment as
269 compared to the other three depths with a minimum (0.8 dS/m) and maximum (33.3 dS/m),
270 however the mean EC_e was largest (17.4 dS/m). This constrains the EC_e data and means that the

efficiency of the model will be somewhat compromised. This was the case as this model was then most inefficient (0.66) with the largest RMSE (7.58 dS/m).

In terms of EC_a, the model result for the subsoil depth was also impacted by the fact that the EC_a was most likely influenced by the more conductive topsoil and subsurface salinity, particularly in the areas where the EC_e was at a maximum. This leads to much of the secondary magnetic field to be channeled near the surface and therefore measurement to deeper depths is compromised.

Semi-variogram analysis

The fitted semi-variogram models of the measured apparent soil electrical conductivity (EC_a) for both the EC_{ah} and EC_{av} are shown in Fig. 5a. For both EC_a, a spherical model best fitted the data. The EC_{ah} semi-variogram has a larger nugget (1.2×10^{-4}) compared with EC_{av} (0.8×10^{-4}). The range was approximately 60 m for both EC_a. Equivalent variograms were generated for the estimated soil electrical conductivity of a saturated soil paste extract (EC_e) for each of the depths of interest (Fig. 5b).

The nugget (C_0) to Sill (C_0+C) ratio is often used to characterize short distance auto correlation and spatial dependence of the variables (Gorai *et al.*, 2017). According to Camberdella *et al.*, (1994), a nugget: sill ratio less than 25% is indicative of strong spatial dependence while values between 25-50% and more than 75 are representative respectively of moderate and weak spatial dependence. Utilizing these indices in this study, it was found that estimated EC_e had strong (22.5%) spatial dependency.

Despite this, and owing to the presence of a nugget variance, improvements in semi-variogram development and to better predict EC_e measurements of EC_a could be made at smaller

grid spacing approximately only 1 m apart. This could be facilitated by mobilizing the EM38 onto a small sled capable of being dragged behind a small all-terrain vehicle or even by hand. Herein this was difficult owing to various crops being present and at various stages of growth.

Measured versus predicted EC_e

Fig. 6(a-c) shows a plot of predicted versus measured EC_e for all depths, achieved using a leave one-out-cross-validation (LOOCV) procedure. It was evident, for the most part, that the predicted EC_e achieved from the MLR modelling (calibration) and kriging (interpolation) was successful and generally fall close to the 1:1 line (Fig. 6a). We describe the results with reference to the salinity classes defined by Barrett-Lennard *et al*., (2008).

This was the case for calibration locations where the measured EC_e was small and either non-saline (< 2 dS/m) to only slightly-saline (2-4 dS/m). This was the case at sample site 256. Fig. 6b shows that for this salinity profile, measured EC_e was uniformly non-saline, excepting the topsoil which was moderately saline (4-8 dS/m). Our ability to predict EC_e at all depths, except the topsoil, and as shown in Fig. 6c, indicates that our calibration and interpolation was satisfactory in this instance. This indicates some confidence in prediction of non-saline conditions along the eastern margin.

This was also the case for predicted EC_e, which was intermediate, as exemplified by calibration site 177. Located to the north of site 256, the essentially normally distributed salinity profile; whereby EC_e increases with increasing depth as a logistic curve (Triantafilis *et al*., 2000), was for the most part well predicted in the topsoil and subsoil depths (i.e. >0.9 m).

However, and as shown in Fig. 6c, the lower topsoil (0.15-0.3 m) and subsurface (0.3-0.6 m) EC_e were measured as being highly-saline (8-16 dS/m) but were slightly over-predicted as

317 severely-saline (16-32 dS/m). We attribute this to the short scale variation in EC_a around site
318 177, which was intermediate-large (300-400 mS/m) along a narrow band and as shown in Fig.
319 4b.

320 As measured EC_e increased to much larger values, for example at site 105, our ability to
321 predict EC_e was also reasonable, despite the extremely-saline EC_e (> 32 dS m^{-1}). In this inverted
322 salinity profile, located along the southern margin of the farm, measured salinity (51 dS/m)
323 decreased from the topsoil to the subsoil (0.6-0.9 m), where EC_e was still extreme. At most depth
324 increments, predicted EC_e was equivalent (Fig. 6c). Given the salinity profile was inverted, this
325 suggests that the process of secondary salinization was being driven by strong evaporative
326 demand, capillary rise and from the presence of the water table; which was saline given the
327 extreme EC_e.

328 There were, however some instances where measured and predicted EC_e were not
329 consistent. This was the case at site 40, which was in the northeast corner of the farm. From Fig.
330 4(a and b) it was apparent that the site was in an area where measured EC_{ah} and EC_{av} were small
331 (<200 mS/m). This was generally consistent with the small measured EC_e, which was non-saline
332 in the topsoil and only slightly saline at lower depth increments (Fig. 6b). This was not the case,
333 however, regarding the predicted EC_e (Fig. 6c), which suggested EC_e was highly saline (8-16
334 dS/m) to severely saline EC_e (16-32 dS/m).

335 While the calibration was satisfactory, and as indicated by the good results achieved by
336 the LOOCV during calibration, here where we also consider the interpolation of the EC_e data
337 predicted. Specifically, where the EC_a data was collected at the 276 measurement sites, the
338 predicted EC_e is a function of the short scale variation. It was also a function of the survey
339 interval of approximately 15 m transects and measurement spacing shown in Fig. 2a. As a result,

and in the northeast part of the study area EC_a changed from small to intermediate values of EC_a over a short distance. Consequently, EC_e was over-predicted. The opposite was the case at site 50; whereby predicted EC_e was under-predicted.

To better predict EC_e, particularly considering the small scale spatial variation in EC_a and apparent in Figure 4a and 4b, EM38 should be collected at smaller grid spacing. Whilst using a MESS (Mobile electromagnetic sensing system) is preferred, the size of the farms and the individual fields most likely precludes this in developing countries. An alternative is to mount an EM38 onto a small sled along with a GPS and data logger and dragging the sled by hand to allow for the collection of continuous data (Koganti *et al.,* 2018). This would also require upgrading the EM38, used herein, to record digital data.

Digital Soil Maps of EC_e

Fig. 7 and 8 show the DSM developed from the MLR models (developed at the 21 calibration sties) and interpolated using ordinary kriging from the predicted EC_e at the 276 EC_a survey locations. Fig. 7a and 7b show the DSM for the upper (0-0.15 m) and lower (0.15-0.30 m) topsoil. These DSM show clearly that few areas on the farm were not affected by some form of salinization. In terms of the upper topsoil, the areas which were relatively unaffected were located along the eastern margin and the northeast corner of the farm. Here, in an area less than 3 % of the farm, EC_e was only slight to moderately saline (< 8 dS/m). At these levels, wheat (*Triticum aestivum L.*) which is sometimes grown in adjacent farms, could reasonably be expected to at least germinate, however the threshold EC_e (6 dS/m) was exceeded (Maas and Hoffman, 1977). This explains why it is seldom grown as a staple crop.

Across a much larger part of the farm, the EC_e was highly-saline (8-16 dS/m) across 35.4%. This was predominantly situated in the western part of the farm. Here, the impact of salinity begins to become problematic at the time of germination because the main crop which is grown in the winter is Indian mustard (*Brassica Juncea)*, which although moderately salinity tolerant, its thresholds were exceeded in most parts of this area (9 dS/m). This explains why this farm was abandoned by the farmer in the early 1980's.

The reason it was abandoned becomes self-explanatory given more than half of the farm (55.4%) has been mapped as severely-saline (16-32 dS/m) with a smaller area (6.3%) extremely-saline (> 32 dS/m). In both cases, these values characterize the southern half of the farm (Fig. 7 and 8). Here, the tell-tale signs of extremely saline soil conditions are evident year-round. During the monsoonal period (July to mid-September), when the water table is within 1 m, water logging and presence of a saline water table is problematic. During the summer, when the water table is around 3 m deep, the high evaporative demand of plants and evaporation leave salt crystals on the surface. The reason for these problems is because the southern part of the farm is situated in a depression.

In terms of management there are various options, including crop, soil and water management. These will need to be considered in combination, considering the severely to extremely saline nature of salinity. In terms of crop management, salt tolerant crops (e.g. barley) and salt tolerant variety need to be considered. Forestry plantation (Eucalyptus) was also planted for controlling shallow saline water table and to generate income. To enable more effective water management, pressurised irrigation techniques (drip and sprinkler) and installation of sub surface drainage to lower the shallow saline water table and facilitate leaching of salts during the wet season need to be considered. Soil management could include the preparation of beds that

encourage salts to accumulate in areas away from germinating seedlings; when salinity is most problematic.

Summary and Conclusions

The effective control of soil salinity requires knowledge of its magnitude and extent. In this paper, we demonstrated how this could be done using a simple to use geophysical instrument (EM38) on an approximate regular grid. By considering EC_a in the horizontal (EC_{ah}) and vertical (EC_{av}) modes and considering two trend surface parameters (Easting and Northing), we could use two modules in an easy to use software package (ESAP) to first determine a suitable number of soil sample locations (RSSD) and then predict EC_e at the EC_a measurement sites using a MLR. Using ordinary krigging (OK) interpolation method spatial distributions of EC_e were predicted for top, subsurface and subsoil depths and DSM of soil salinity was prepared.

The DSM of soil salinity at two topsoil (0-0.15 m) and (0.15-0.30 m) a subsurface (0.3-0.6) and a subsoil (0.6-0.9) depths can act as baseline information which can be used to gauge the impact of soil, water and crop management introduced to manage salinity. Improvements in the DSM however need to be sought. In the first instance, to account for the short scale spatial variation of EC_e, a small sled capable of being dragged behind a small all-terrain vehicle or even by hand needs to be designed and developed to mobilise the EM38 and GPS and to enable higher resolution EC_a data.

The collection of higher resolution GPS data in the vertical orientation (i.e. height) might allow for improved prediction of EC_e, particularly in the depressed areas in the southern part of the farm. With higher resolution EC_a data it might also be possible to better model the EC_e data by modelling this data directly from the estimated true electrical conductivity using inversion

software (e.g. EM4soil). This is because soil salinity with depth has been shown to be more easily and more efficiently using a single calibration equation in 2-dimensions (Stockman *et al.*, 2017), at the field scale (Zare *et al*., 2015) and at the district level (Dadak *et al.*, 2017).

References

ArcGIS 9.3. 2008**.** ArcGIS 9.3 Improves Your Entire GIS Workflow**.** ESRI Press Release. http://www.esri.com/news/releases/08_2qtr/arcgis_9_3.html.

Aziz, Z., van Geen, A., Stute, M., Versteeg, R., Horneman, A., Zheng,Y., Goodbred, S., Steckler, M., Weinman, B., Gavrieli, I., Hoque, M. A., Shamsudduha, M. & Ahmed, K. M. 2008. Impact of local recharge on arsenic concentrations in shallow aquifers inferred from the electromagnetic conductivity of soils in Araihazar, Bangladesh. *Water Resources Res*earch, 44, W07416, doi:10.1029/2007WR006000

Banerjee, S., Das, D.K., Yadav, B.R., Gupta, N., Chandrasekharan, H., Ganjoo, A.K. & Singh, R. 1998. Estimation of soil salinity at IARI farm by Inductive Electro- magnetic technique. *Journal of Indian Society of Soil Science*, **46**, 110-115.

Barrett-Lennard, E.G., Bennett, S.J. & Colmer, T.D. 2008. Standardising the terminology for describing the level of salinity in soils. In: Proceedings of the 2nd International Salinity Forum: Salinity, Water and Society-Global Issues, Local Action, Adelaide, SA, Australia, 31 Mar.-3 Apr. 2008. *Geological Society of Australia*, Hornsby, NSW, Australia.

Bhargava, G.P. 2003. Training manual for undertaking studies on genesis of sodic /alkali soils. Technical Bulletin: CSSRI/Karnal/ 2003/, pp-111.

Brevik, E.C., Fenton, T.E. & Lazari, A. 2006. Soil electrical conductivity as a function of soil water content and implications for soil mapping. *Precision Agriculture*, 7, 393–404.

Buchanan, S.M. & Triantafilis, J. 2009. Mapping water table depth using geophysical and environmental variables. *Ground Water*, **47**, 80–96.

Cambardella, C.A., Moorman, T.B., Novak, J.M., Parkin, T.B., Turco, R.F. & Konopka, A.E. 1994. Field-scale variability of soil properties in central Iowa soils. *Soil Sci. Soc. Am. J.*, **58**, 1501–1511.

Cassel, F., Goorahoo, D. & Sharmasarkar, S. 2015. Salinization and Yield Potential of a Salt-Laden Californian Soil: an In Situ Geophysical Analysis. *Water Air and Soil Pollution*, **226**, 422.

Chaudhary, M.R & Baig, A. 2000. Electromagnetic Induction Device (EM38) Calibration an Monitoring Soil Salinity/Environment (Pakistan); Vlotman, W.F., Ed.; EM38 Workshop: New Dehli, India, 2000; pp. 37–48.

Dadak, H., Huang, J., Zouahri, A., Douaik, A., Triantafilis, J., 2017. Mapping soil salinity in 3-dimensions using an EM38 and EM4Soil inversion modelling at the multi-farm scale in central Morocco. *Soil Use and Management*, 33, 553-567.

Friedman, S.P. 2005. Soil properties influencing apparent electrical conductivity: A review. *Computer and Electronics in Agriculture*, **46**, 45–70.

Gorai, T., Ahmed, N., Patra, A.K., Sahoo, R.N., Sarangi, A., Meena, M.C. & Sharma, R.K. 2017. Site Specific Nutrient Management of an Intensively Cultivated Farm Using Geostatistical Approach. *Proc. Natl. Acad. Sci., India, Sect. B Biol. Sci*., **87 (2)**, 477-488.

451 Herrero, J., Netthisinghe , A., Hudnall, W.H. & Pérez-Coveta, O. 2011. Electromagnetic
452 induction as a basis for soil salinity monitoring within a Mediterranean irrigation district.
453 *Journal of Hydrology*, **405**, 427–438.
454 Huang, J., Wong, V. N. L. & Triantafilis, J. 2014. Mapping soil salinity and pH across an
455 estuarine and alluvial plain using electromagnetic and digital elevation model data. *Soil*
456 *Use Management*, **30**, 394–402.
457 Kamra, S.K. 2015. An overview of subsurface drainage for management of waterlogged saline
458 soils of India. *Water and Energy International*, **58**, 46-53.
459 Koganti, T., Najary, B., Pathan, A., Huang, J., Triantafilis, J. 2018. Mapping soil salinity in a
460 highly salinized field using quasi-3d electromagnetic conductivity imaging. *Land*
461 *Development and Degradation*, *DOI: 10.1002/ldr.2973*.
462 Kumar, R., Ghabru, S.K., Singh, N.T., Ahuja, R.L. & Sharma, B.D. 2010. Origin of salinity in
463 the Indus plains of the Indian sub-continent. *Journal of soil salinity and water quality*,
464 **2(1)**, 24-33.
465 Lesch, S. M., Rhoades, J. D. & Corwin, D. L., 2000. The ESAP-95 version 2.01R user manual
466 and tutorial guide. Research Report No. 146. USDA-ARS, George E. Brown, Jr.,
467 Salinity Laboratory, Riverside, California.
468 Lesch, S.M., Strauss D.J. & Rhoades J.D. 1995b. Spatial prediction of soil salinity using
469 electromagnetic induction techniques: 2. An efficient spatial sampling algorithm suitable
470 for multiple linear regression model identification and estimation. *Water Resources*
471 *Research*, **31**, 387-398.
472 Li, H.Y., Shi, Z., Webster, R. & Triantafilis, J. 2013. Mapping the three-dimensional variation of
473 soil salinity in a rice-paddy soil. *Geoderma*, **195-196**, 31–41.

Li, X.M., Yang J.S., Liu M.X., Liu, G.M. & Yu, M. 2012. Spatio-Temporal Changes of Soil Salinity in Arid Areas of South Xinjiang Using Electromagnetic Induction. *Journal of Integrative Agriculture*, **11(8)**, 1365-1376.

Maas, E.V. & Hoffman, G.J. 1977. Crop salt tolerance - current assessment. *Journal of the Irrigation and Drainage Division*, **ASCE 103 (IR2),** 115-134.

Mandal, A.K., Sethi, Madhurama, Yaduvanshi, N.P.S., Yadav, R.K., Bundela, D.S., Chaudhari, S.K., Chinchmalatpure, A. & Sharma, D.K., 2013. Salt Affected Soils of Nain Experimental Farm: Site Characteristics, Reclaimability and Potential Use. Technical Bulletin: CSSRI/Karnal/ 2013/03, pp-34

Mckenzie, R.C., Chomistek, W. & Clark, N.F. 1989. Conversion of electromagnetic inductance readings to saturated paste extract values in soils for different temperature, texture, and moisture conditions. *Canadian Journal of Soil Science*, **69**, 25-32.

Nagra, G., Burkett, D., Huang, J., Ward, C. & Triantafilis, J. 2017. Field level digital mapping of soil mineralogy using proximal and remote-sensed data. *Soil Use and Management*, **33**, 425–436.

Narjary, B., Jangra, P., Abhishek, R., Kumar, N., Raju, R., Thimappa, K., Meena, R.L., Kumar, S., Kumar, P., Chichmatalpure, A.R. & Kamra, S.K. 2017. Quantitative assessment of soil salinity using electromagnetic induction technique and geostatistical approach**.** *Journal of Soil Salinity and Water Quality*, **9,** 156-166.

Odeh I.O.A., Todd A.J., Triantafilis, J., McBratney, A.B., 1998. Status and trends of soil salinity at different scales: the case of the irrigated cotton growing region of eastern Australia. *Nutrient Cycling in Agroecosystems*, **5,** 99-107.

496 Rhoades, J.D., Chanduvi, F. & Lesch, S. 1999. Soil salinity assessment: methods and
497 interpretation of electrical conductivity measurements. FAO Irrigation and Drainage
498 Paper 57. Food and Agriculture Organization of the United Nations, Rome, Italy, pp. 1–
499 150.
500 Sachdev, C.B., Lal, T., Rana, KP.C. & Sehgal, J. 1995. Soils of Haryana for Optimizing Land
501 Use. *NBSS Publ.* 44 *(Soils of India Series* 3), National Bureau of Soil Survey and Land
502 Use Planning, Nagpur, India, pp. 59.
503 Saey, T., Simpson, D., Vermeersch, H., Cockx, L. & Van Meirvenne, M. 2009. Comparing the
504 EM38DD and DUALEM-21S sensors for depth-to-clay mapping. *Soil Science Society of*
505 *America Journal*, **73**, 7–12.
506 Srivastava, P., Pal, D.K., Aruche, K.M., Wani, S.P. & Sahrawat, K.L. 2015. Soils of the Indo-
507 Gangetic Plains: a pedogenic response to landscape stability, climatic variability and
508 anthropogenic activity during the Holocene. Earth Science Reviews, **140,** 54–71.
509 Stockmann, U., Huang, J., Minasny, B. & Triantafilis, J. 2017. Utilizing a DUALEM-421 and
510 inversion modelling to map baseline soil salinity along toposequences in the Hunter
511 Valley Wine district. *Soil Use and Management*, **33,** 413-424.
512 Triantafilis, J. & Lesch, S.M. 2005. Mapping clay content variation using electromagnetic
513 induction techniques. *Computers and Electronics in Agriculture*, **46**, 203-237.
514 Triantafilis, J., Laslett, G.M. & Mcbratney, A.B. 2000. Calibrating an electromagnetic induction
515 instrument to measure salinity in soil under irrigated cotton. *Soil Science Society of*
516 *America Journal*, **64**, 1009–1017.

Triantafilis, J., Wong, V., Santos, F.A.M., Page, D. & Wege, R. 2012. Modeling the electrical conductivity of hydrogeological strata using joint-inversion of loop-loop electromagnetic data. *Geophysics***,** 77 **(4)**, WB99–WB107.

Vaughan, P.J., Lesch, S.M., Corwin, D.L. & Cone D.G. 1995. Water content effect on soil salinity prediction: a geostatistical study using cokriging. *Soil Science Society of America Journal*, **59**, 1146-1156.

Zare, E., Huang, J., Monteiro Santos, F.A. & Triantafilis, J. 2015. Mapping Salinity in Three Dimensions using a DUALEM-421 and Electromagnetic Inversion Software. *Soil Science Society of America Journal*, **79**, 1729-1740.

Table 1: Descriptive statistics of EM38 in horizontal ($EM38_H$) and vertical $EM38_V$ (mS/m), Electrical conductivity of saturated soil paste extract (EC_e - dS/m), Saturation percentage (SP, %), gravimetric moisture content (GMC, %), calcium and magnesium concentration in saturation extract (Ca+Mg, meq/l), Sodium and K concentration in saturation extract (Na and K, meq/l), Carbonate and bicarbonate concentration in saturation extract (CO_3+HCO_3, meq/l) Chlorine concentration in saturation extract (Cl, meq/l).

Parameters	**n**	**Mean**	**SD**	**Minimum**	**Maximum**	**Skewness**	**Kurtosis**
EC_a (Survey)							
EM_H	276	358.3	182.1	45.0	962.0	0.5	-0.4
EM_V	276	404.7	162.0	58.0	771.0	0.1	-0.7
EC_a (Calibration)							
EM_H	21	324.7	182.1	45.0	804.0	0.9	0.1
EM_V	21	367.9	197.3	58.0	752.0	0.3	-0.9
Soil Properties							
EC_e (0-0.15 m)	21	16.7	15.1	2.0	50.8	1.1	0.2
EC_e (0.15-0.3 m)	21	15.3	11.9	1.3	41.5	0.9	-0.1
EC_e (0.3-0.6 m)	21	16.5	11.3	1.0	38.1	0.4	-0.5
EC_e (0.6-0.9 m)	21	17.4	11.6	0.8	33.3	0	-1.6
SP (0-0.15 m)	21	47.0	1.0	44.5	48.8	-0.8	1.4
SP (0.15-0.3 m)	21	46.5	1.8	42.9	49.7	-0.5	-0.3
SP (0.3-0.6 m)	21	46.3	1.0	43.5	48.1	-0.7	1.7
SP (0.6-0.9 m)	21	46.3	0.9	44.6	47.7	-0.7	-0.6
GMC (0-0.15 m)	21	14.4	3.7	8.5	22.7	0.3	-0.4
GMC (0.15-0.3 m)	21	16.7	2.8	10.6	22.0	0	0.4
GMC (0.3-0.6 m)	21	18.8	3.1	14.1	28.0	1.3	2.7
GMC (0.6-0.9 m)	21	19.9	2.8	14.6	25.0	0.4	-0.1
Na (0-0.15 m)	21	199.6	207.8	6.0	659.4	1	-0.2
Na (0.15-0.3 m)	21	149.3	143.9	4.3	492.5	1.3	0.8
Na(0.3-0.6 m)	21	173.0	145.2	3.0	470.0	0.7	-0.3
Na(0.60-0.9 m)	21	203.9	157.8	4.6	504.0	0.3	-1
Cl (0-0.15 m)	21	122.9	108.4	5.2	369.9	0.8	-0.4
Cl (0.15-0.3 m)	21	92.3	81.6	4.7	263.2	0.9	-0.3
Cl(0.3-0.6 m)	21	92.8	77.2	5.2	238.3	0.7	-0.9
Cl (0.6-0.9 m)	21	114.1	81.8	17.4	249.1	0.3	-1.6
Ca+Mg (0-0.15 m)	21	50.0	43.7	4	210	2.6	8.9
Ca+Mg (0.15-0.3 m)	21	38	30.2	6	120	1.1	1
Ca+Mg (0.30-0.6 m)	21	39.4	34.3	7	120	1	-0.2
Ca+Mg (0.6-0.9 m)	21	38.3	36.1	8	141	1.5	1.9
CO_3 + HCO_3(0-0.15 m)	21	2.7	0.9	1.4	5.2	1.7	3.3
CO_3 + HCO_3(0.15-0.3 m)	21	2.7	0.9	1	4.8	0.2	0
CO_3 + HCO_3(0.3-0.6 m)	21	2.6	0.6	1.7	4.2	0.7	1.2
CO_3 + HCO_3(0.6-0.9 m)	21	2.6	0.8	1	4.3	0.1	0.1
K (0-0.15 m)	21	0.95	0.15	0.04	2.86	0.98	1.36
K (0.15-0.3 m)	21	0.57	0.1	0.09	1.84	1.55	2.1
K (0.3-0.6 m)	21	0.55	0.14	0.08	2.86	2.77	9.53
K (0.6-0.9 m)	21	0.44	0.11	0.08	2.16	2.61	7.85

Table 2: Pearson correlation analysis among apparent conductivities (V and H) and soil properties for average soil profile (0-90 cm) including the electrical conductivity of saturated soil paste extract (EC_e - dS/m), saturation percentage (SP, %), gravimetric moisture content (GMC, %), and from the saturated extract the sodium and K (Na and K, meq/l), chloride (Cl, meq/l), calcium and magnesium (Ca+Mg, meq/l), and arbonate and bicarbonate (CO_3+HCO_3, meq/l).

	V	*H*	*EC_e*	*SP*	GMC	*Na*	*Cl*	*Ca+Mg*	CO_3+HCO_3
H	0.90**								
EC_e	0.74**	0.76**							
SP	0.03	-0.03	0.06						
GMC	-0.22	-0.23	-0.05	0.31					
Na	0.74**	0.77**	0.93**	0.29	0.01				
Cl	0.71**	0.73**	0.83**	0.18	-0.03	0.81**			
Ca+Mg	0.37	0.37	0.43	-0.10	-0.04	0.26	0.70**		
CO_3+HCO_3	-0.26	-0.21	-0.12	-0.06	0.21	-0.07	-0.39	-0.57*	
K	0.41	0.37	0.62*	-0.06	-0.24	0.50*	0.60*	0.63*	-0.23

** Significant at $p< 0.01$ and * significant at $p<0.05$

Table 3. Multiple linear regression (MLR) models for estimating saturated paste electrical conductivity (EC_e), based from electromagnetic induction (EM) readings in horizontal (EC_{ah}) and vertical (EC_{av}) and two trend surface parameters (i.e. Easting and Northing) for the upper (0 – 0.15 m) and lower topsoil (0.15-0.3 m), subsurface (0. 30-0.6 m) and subsoil (0.6-0.9 m) depths.

Parameter	Model details	0-15 cm	15-30 cm	30-60 cm	60-90 cm	Average 0-90cm
EC_e	Model Selected	$EC_e = b0 + b1(z1) + b2(z1^2) + b3(x) + b4(x^2)$				
	Model R^2	0.86	0.77	0.78	0.66	0.84
	RMSE	6.36	6.32	5.96	7.58	5.01
	Model Efficiency	0.86	0.77	0.72	0.66	0.79
	Index of Aggrement	0.96	0.93	0.91	0.89	0.94

Where,

b, b1, b2, b3, and b4 are coefficients;

z1 = decorelated signals;

x = trend surface parameter

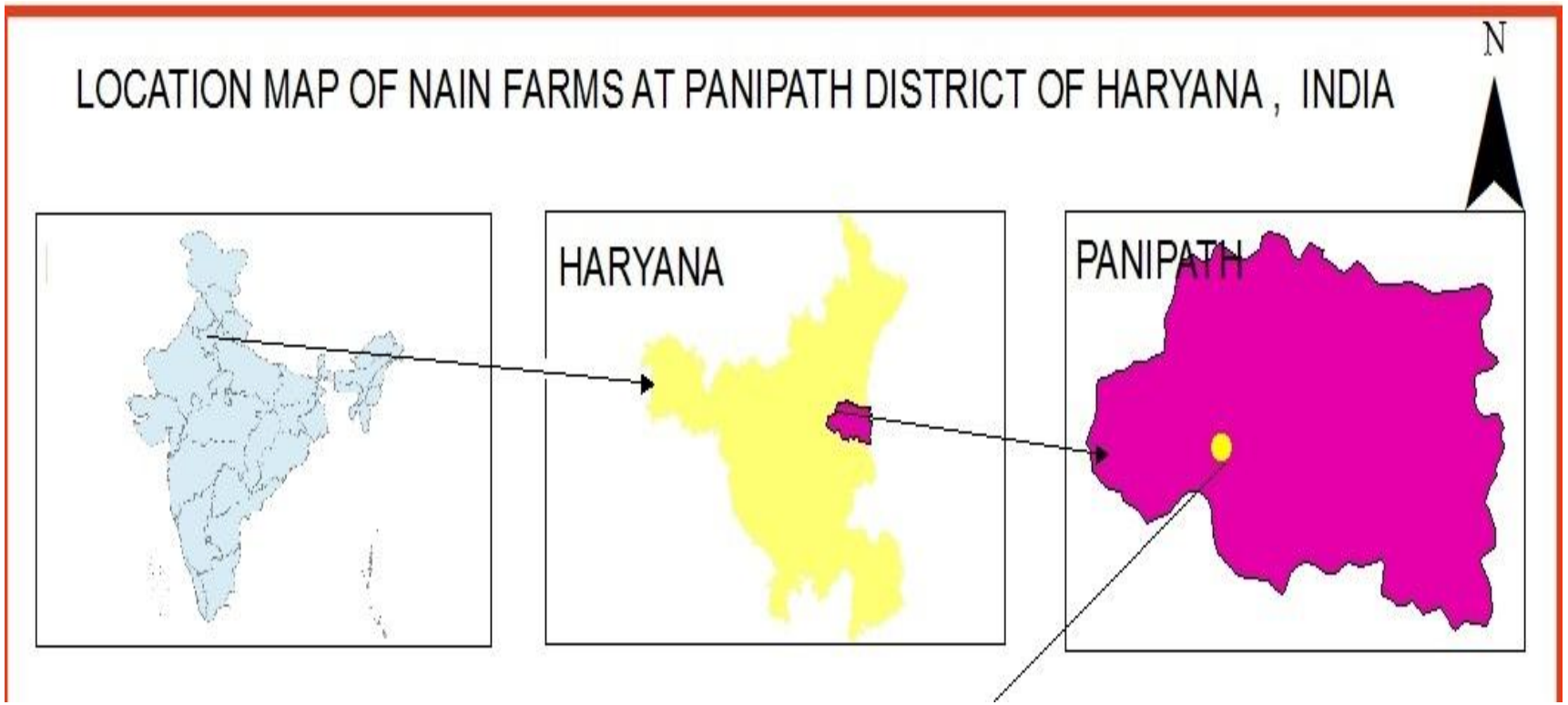

Fig 1: Location map of experimental farm (Nain, Panipat, Haryana, India)

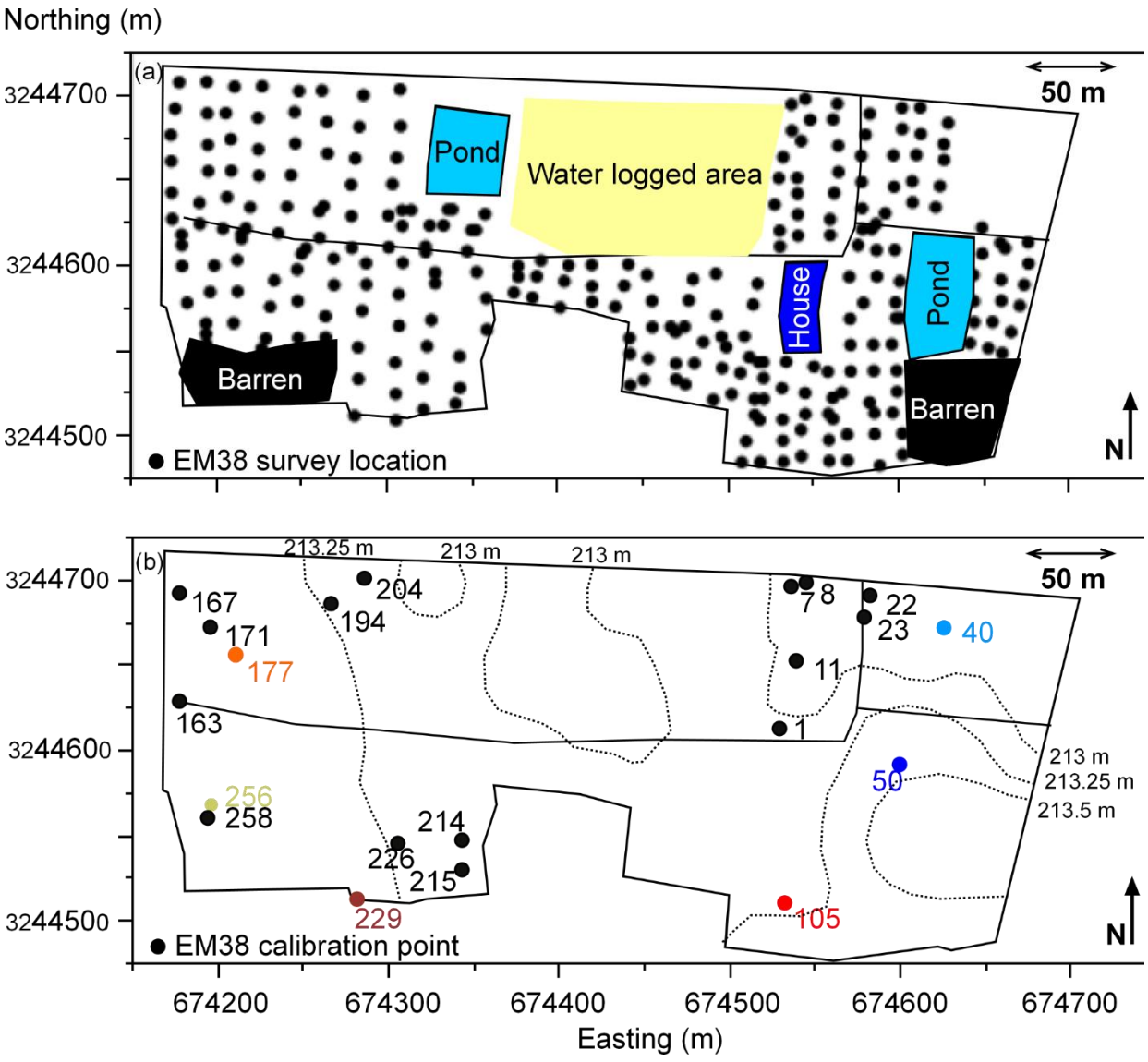

Fig.2: Spatial distribution of (a) EM38 survey locations and (b) EM38 calibration points across the experimental farm (Nain, Panipat, Haryana, India. Note: Dotted lines represent elevation (above mean sea level – m).

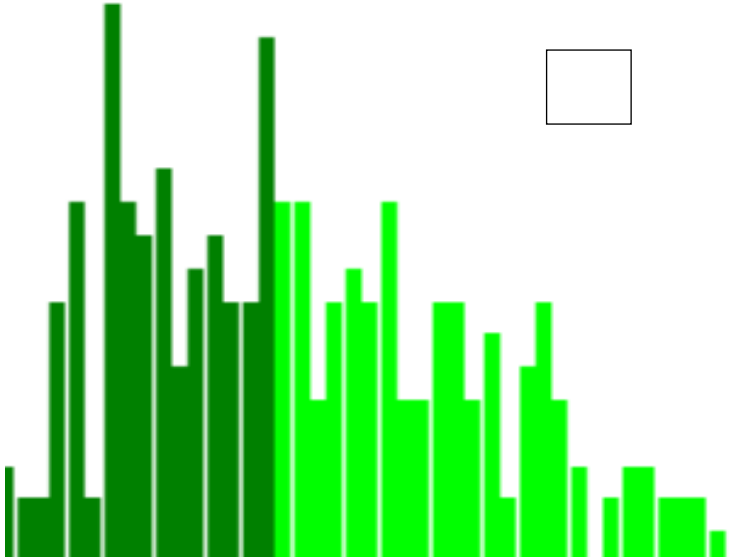

Fig.3a: Signal histogram in $EM38_h$ measurements

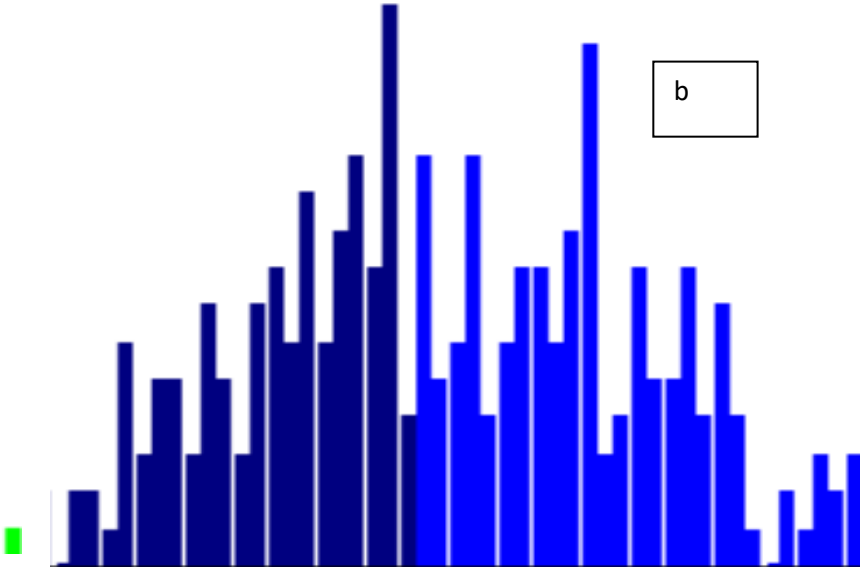

Fig.3b: Signal histogram in $EM38_v$ measurements

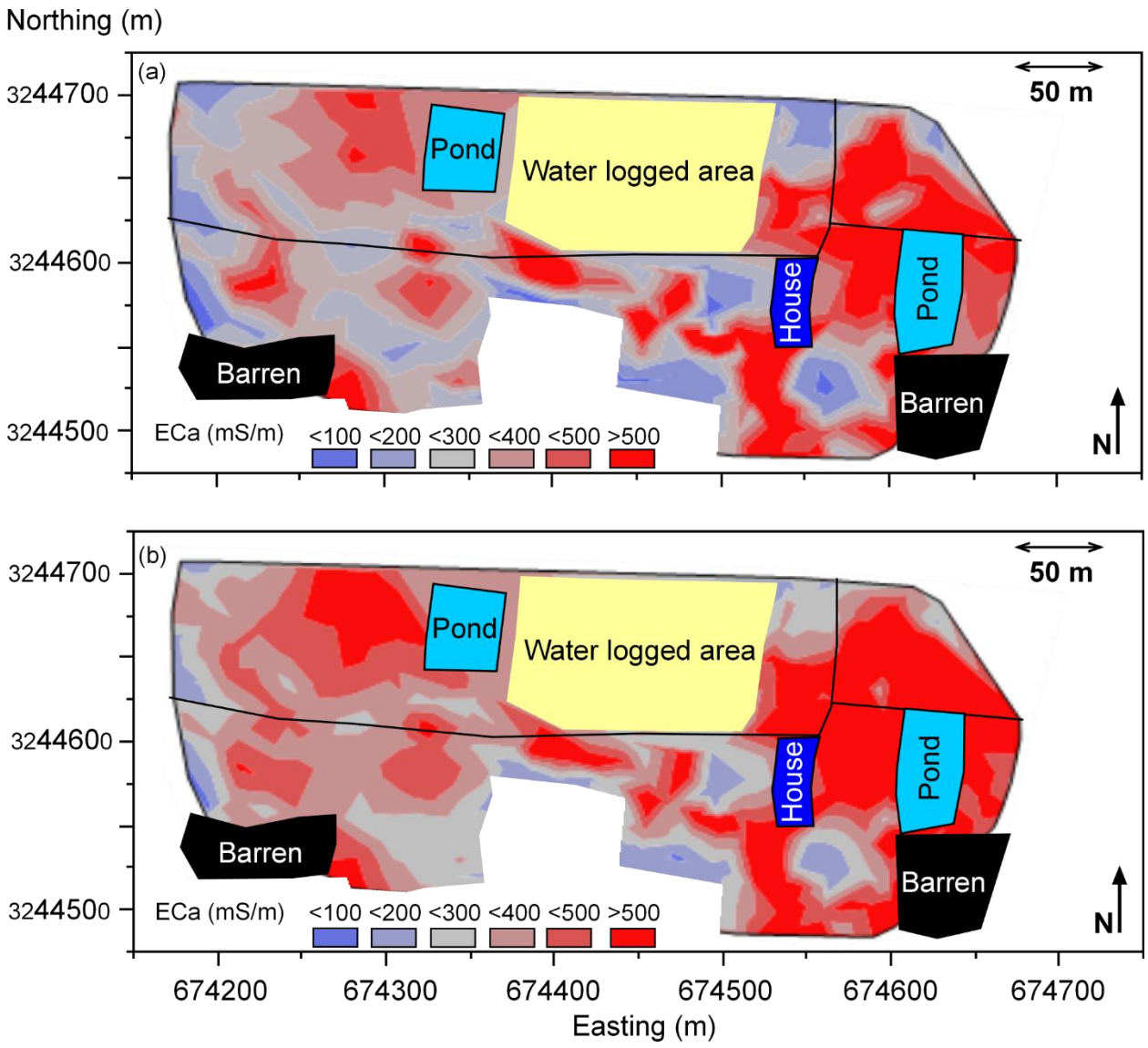

Fig 4: Contour plot of measured soil apparent electrical conductivity (EC_a – mS/m) using an EM38 in (a) horizontal (EC_{ah}) and (b) vertical (EC_{av}) modes of operation

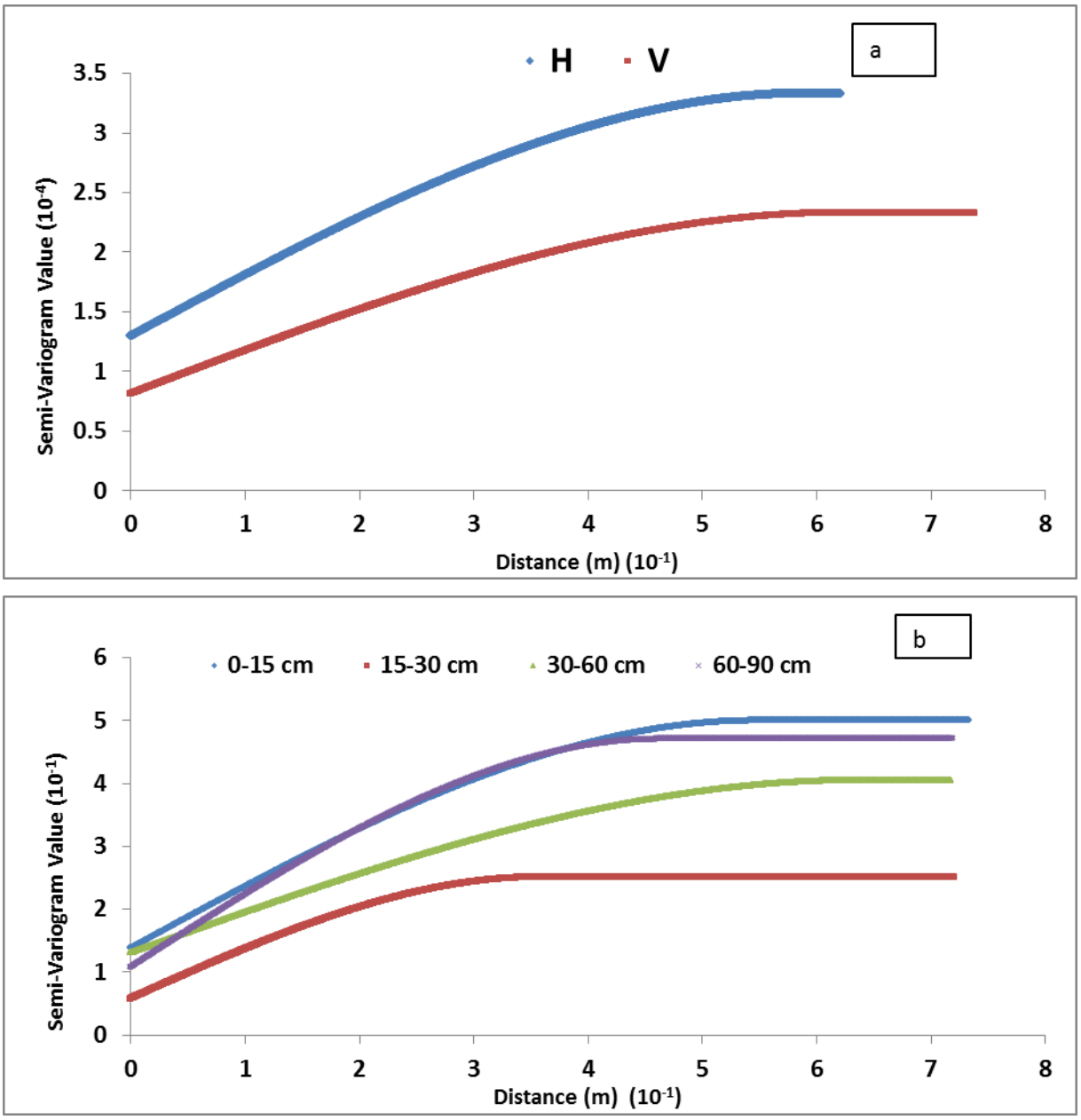

Fig. 5 Semi-variograms a) measured soil apparent electrical conductivity (EC_a – mS/m) using an EM38 in horizontal (EC_{ah}) and vertical (EC_{av}) modes of operation and b) estimated electrical conductivity of a saturated soil paste extract (EC_e – dS/m) at depth increment of topsoil (0-0.15 m), subsurface (0.15-0.3 m) and upper (0.3-0.6 m) and lower (0.6-0.9 m) subsoil.

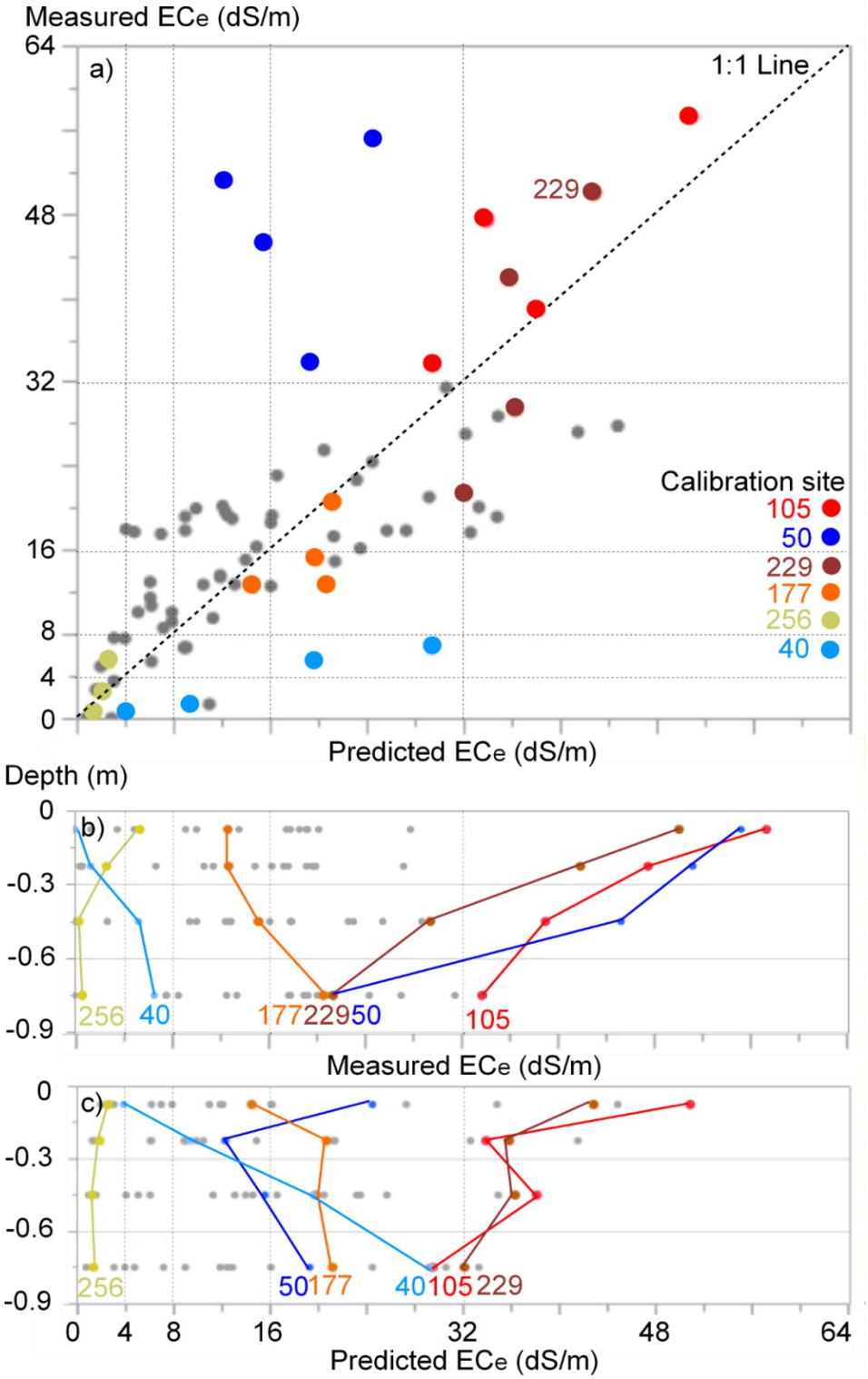

Fig. 6. Plot of a) predicted versus measured electrical conductivity of a saturated soil paste extract (EC_e - dS/m), b) measured EC_e (dS/m) and depth and c) predicted EC_e (dS/m) and depth.

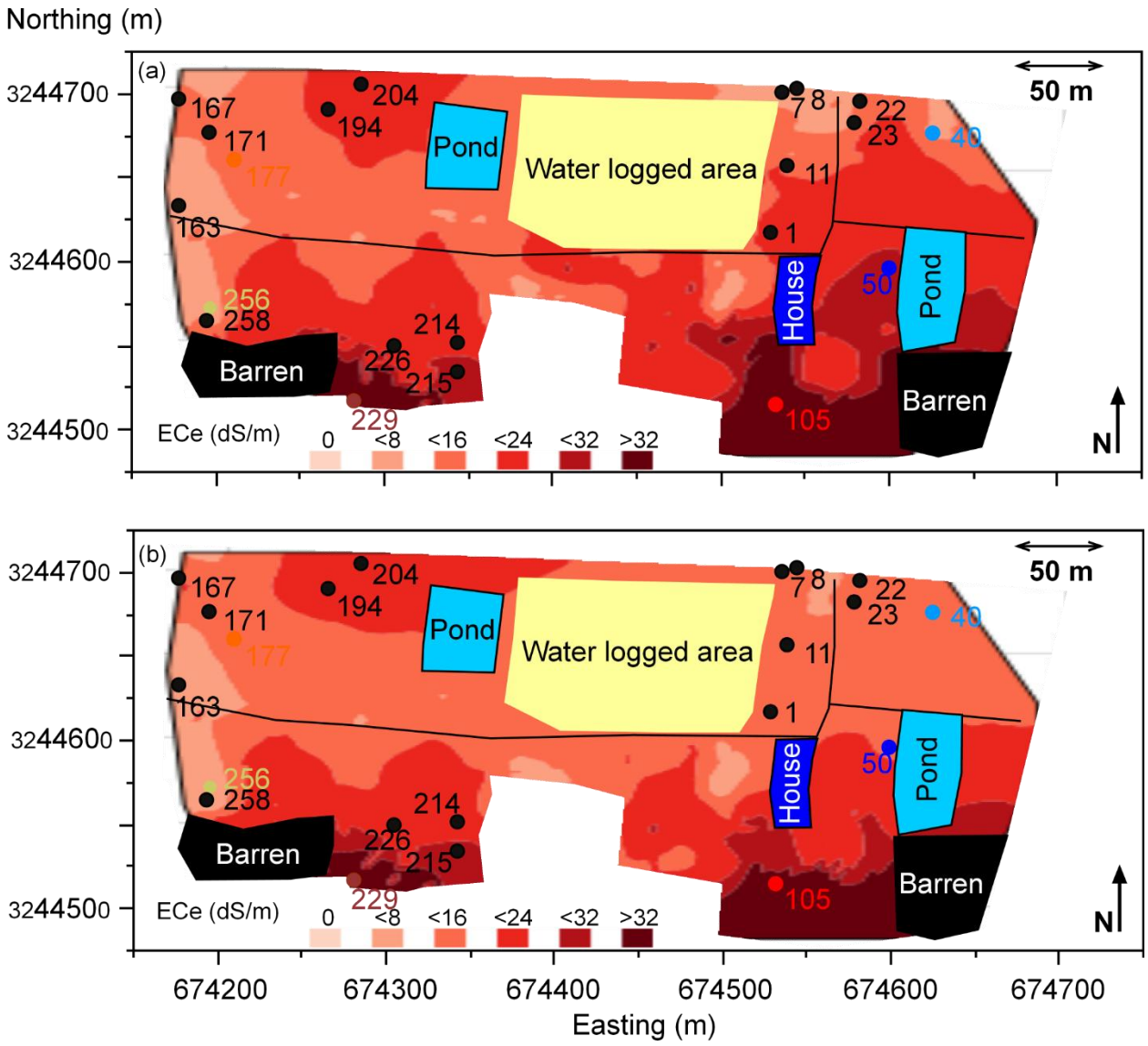

Fig. 7 Contour plot of kriged estimated electrical conductivity of a saturated soil paste extract (EC_e – dS/m) at depth increments of a) topsoil (0-0.15 m), and b) subsurface (0.15-0.3 m).

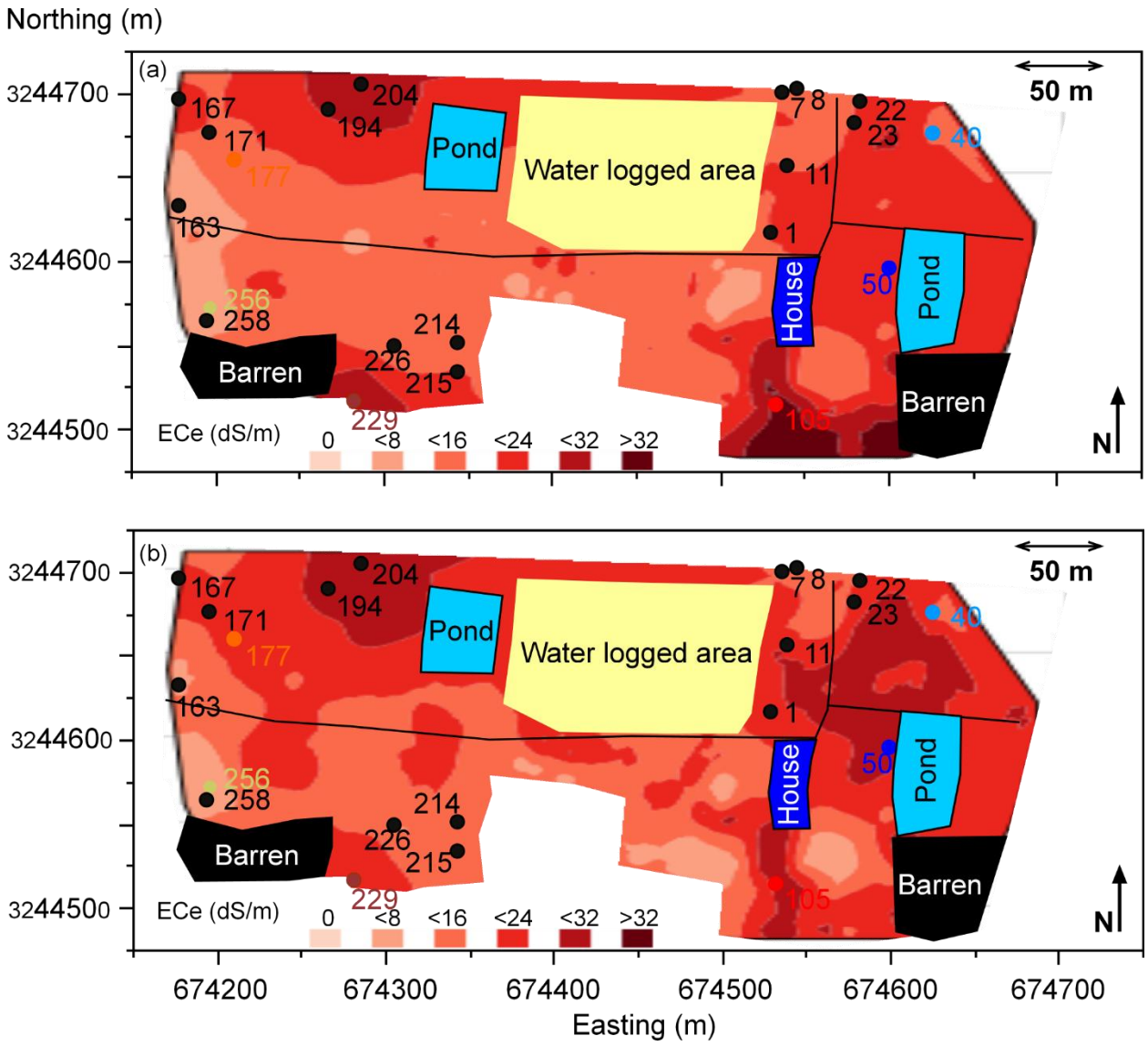

Fig. 8 Contour plot of kriged estimated electrical conductivity of a saturated soil paste extract (EC_e – dS/m) at depth increments of a) upper (0.3-0.6 m), and b) lower (0.6-0.9 m) subsoil.